

Study on the magnetic field strength of NGC 300 ULX1

Y. Y. Pan,^{1*} Z. S. Li,^{1†} C. M. Zhang^{2,3,4} and J. X. Zhong¹

¹Key Laboratory of Stars and Interstellar Medium, Xiangtan University, Hunan 411105, China

²National Astronomical Observatories, Chinese Academy of Sciences, Beijing 100101, China

³CAS Key Laboratory of FAST, Chinese Academy of Sciences, Beijing 100101, China

⁴School of Physical Sciences, University of Chinese Academy of Sciences, Beijing 101400, China

Accepted XXX. Received YYY; in original form ZZZ

ABSTRACT

NGC 300 ULX1 is a pulsating ultraluminous X-ray source (PULX) with the longest spin period of $P \simeq 31.6$ s and a high spin-up rate of $\dot{P} \simeq -5.56 \times 10^{-7} \text{ s s}^{-1}$ that is ever seen in the confirmed PULXs. In this paper, the inferred magnetic field of NGC 300 ULX1 is $\sim 3.0 \times 10^{14}$ G using the recent observed parameters after its first detection of pulsations. According to the evolved simulation of the magnetic field and the spin period, it will become a recycled pulsar or a millisecond pulsar under the conditions of the companion mass and the accretion rate limitation. We suggest that NGC 300 ULX1 is an accreting magnetar accounting for its super Eddington luminosity. We also propose that there might be other accreting magnetars in the confirmed PULXs. Such PULXs will be helpful for understanding the magnetar evolution and the millisecond pulsar formation whose magnetic field is stronger than $\sim 10^9$ G.

Key words: stars: neutron– pulsars: individual: NGC 300 ULX1– stars: magnetic fields– X-rays: binaries.

1 INTRODUCTION

Ultraluminous X-ray sources (ULXs) are the compact objects with the isotropic X-ray luminosity (L_X) higher than $10^{39} \text{ erg s}^{-1}$. They are usually thought as the accreting black holes (BHs) with the stellar or intermediate mass (Miller et al. 2004; Liu & Di Stefano 2008; Roberts et al. 2016). In 2014, M82 X-2 was confirmed to be the first pulsating ULX (PULX) with the detection of a 1.37 s pulsation. It breaks the usual knowledge that ULXs are BHs and indicates there might be more neutron stars (NSs) rather than BHs in ULX populations (Bachetti et al. 2014; Eksi et al. 2015; Shao & Li 2015; King & Lasota 2016; Erkut et al. 2019; King & Lasota 2020).

More than 10 ULXs have been confirmed to be pulsars (PSRs), whose spin-up rate ($|\dot{P}| \sim 10^{-7} - 10^{-10} \text{ s s}^{-1}$) and X-ray luminosity ($L_X \sim 10^{39} - 10^{41} \text{ erg s}^{-1}$) are different with the known accreting NSs (King & Lasota 2020; Song et al. 2020; Erkut et al. 2020). It is suspected that the extraordinary characteristics of PULXs can be understanding through their magnetic field. One interpretation is that PULXs are with fields in the magnetar-level 10^{14} G. Such a strong magnetic field can reduce the electron scattering cross-section and promotes super-Eddington luminosities (Dall’Osso et al. 2015; Eksi et al. 2015; Tong 2015; Pan et al. 2016; Israel et al. 2017). The other explanation is that the magnetic fields of PULXs are in the $10^{12} - 10^{13}$ G range, which matches with the field range of normal pulsars (Bachetti et al. 2014; Fürst et al. 2017; Carpano et al. 2018; King & Lasota 2020). Erkut et al. (2020) found that both magnetar and submagnetar fields were reasonable ($\sim 10^{14}$ G and $\sim 10^{12}$ G), that was with considering a variety of possible spin and luminosity states for each PULX. Moreover, an even low magnetic field

($\sim 10^9$ G) of M82 X-2 had been suggested by Kluzniak & Lasota (2015), which allows the accretion disc extended to the stellar surface. The ultra luminous of PULXs can be attributed to the existence of some degree anisotropy to the radiation field to see the pulsations. A beaming factor can be introduced into the relation between the accretion and isotropic X-ray luminosities as $L_{\text{acc}} = bL_X$, where $b < 1$ (Feng & Soria 2011). However, Mushtukov et al. (2021) found that most confirmed PULXs were with large pulsed fraction and their pulse profiles were nearly sinusoidal, that implied a moderate geometric beaming affection instead of the strong one.

NGC 300 ULX1 is the slowest pulsar with the highest spin-up rate that has ever been observed in the family of known PULXs. According to the observations of *NuSTAR* and *XMM-Newton*, its pulse period, P , spin-up rate, \dot{P} , and luminosity, L_X , are ~ 31.6 s, $\sim -5.56 \times 10^{-7} \text{ s s}^{-1}$, and $\sim 4.7 \times 10^{39} \text{ erg s}^{-1}$ in 0.3 – 30 keV, respectively (Carpano et al. 2018). It has been spun up from ~ 32 s to ~ 20 s within two years after detecting the pulsation (Bachetti et al. 2018; Vasilopoulos et al. 2018). The field strength was derived to be $\sim (0.7 - 10) \times 10^{12}$ G (Vasilopoulos et al. 2018) and $\sim (3 - 20) \times 10^{12}$ G (Carpano et al. 2018) according to the accretion torque on the NS. And based on the accreting model for the magnetar with low magnetic field, it was deduced to be 6.7×10^{13} G (Tong & Wang 2019). Meanwhile, a strong field inferred by Erkut et al. (2020) from the spin-up rate was $(45 - 240) \times 10^{13}$ G. In 2018, Walton et al. (2018) found a cyclotron resonant scattering feature (CRSF) in the spectrum of NGC 300 ULX1 at $E \sim 13$ keV, that illustrated a $\sim 10^{12}$ G magnetic field if it was produced by electron. To account for the high spin-up rate, this CRSF was favored to be produced by proton and implied a magnetar field strength (Erkut 2021). However, Koliopanos et al. (2019) doubted the existence of the CRSF. They introduced a model without the additional absorption feature, which can describe the spectral and temporal characteristics of NGC 300

* E-mail: panyy@xtu.edu.cn

† E-mail: lizhaosheng@xtu.edu.cn

ULX1 successfully. Further detection for the CRSF of NGC 300 ULX1 is needed.

Due to different results and the importance of the magnetic fields in understanding the characteristic of NGC 300 ULX1, in this work, we will study the field strength based on recent observations of the pulse period and spin-up rate. In section 2, the dipole magnetic field of NGC 300 ULX1 is estimated through the torque model by Ghosh & Lamb (1979), hereafter GL model. In section 3, we simulate the evolution of the magnetic field and spin period to inspect the rational field strength for NGC 300 ULX1. The evolved result is studied with the restrictions of the accretion rate and the companion mass. Discussions and conclusions are given in section 4 and 5, respectively.

2 THE MAGNETIC FIELD STRENGTH CALCULATION

2.1 The magnetic field related to the accretion rate

In an accreting binary system, the spin-up rate reflects the angular momentum being deposited on the NS (Shapiro & Teukolsky 1983; Tong 2015)

$$I\dot{\Omega} = -2\pi I \frac{\dot{P}}{P^2} = \dot{M} \sqrt{GMR_A}, \quad (1)$$

where I is the moment of inertia of the NS, $\dot{\Omega}$ is the derivative of the angular velocity, \dot{M} is the accretion rate, G is the gravitational constant, M is the mass of NS, and R_A is the Alfvén radius :

$$R_A = 3.5 \times 10^8 m^{1/7} R_6^{-2/7} L_{37}^{-2/7} \mu_{30}^{4/7} \text{ cm}, \quad (2)$$

where R_6 is the NS radius R in units of 10^6 cm, m is the NS mass in units of solar mass, L_{37} is the accreting luminosity ($L_{\text{acc}} = GM\dot{M}/R$) in units of 10^{37} erg s^{-1} , $\mu_{30} = 1/2 B_{12} R_6^3$ is the magnetic moment in units of 10^{30} G cm^3 , B_{12} is the dipole magnetic field in units of 10^{12} G. With equations (1) and (2), the accretion rate can be written as

$$\dot{M}_{18}^{6/7} \approx -5.1 \times 10^{10} I_{45} m^{-3/7} R_6^{-6/7} P^{-2} \dot{P} B_{12}^{-2/7} \text{ g s}^{-1}, \quad (3)$$

where I_{45} is the moment of inertia I in units of 10^{45} g cm^2 . For a PSR with a certain spin period and spin-up rate, this equation shows an anti-correlation between the accretion rate and the magnetic field. We assume P and \dot{P} of a normal accreting PSR in high mass X-ray binary (HMXB) are ~ 2 s and $\sim -1 \times 10^{-10}$ s s^{-1} , respectively (Liu et al. 2006, 2007). Its $B - \dot{M}$ relation according to equation (3) is shown in the red dotted line in Fig. 1. We see that the magnetic field $\sim 10^{12}$ G of such a PSR corresponds to the accretion rate $\sim 10^{18}$ g s^{-1} . If the magnetic field is as strong as $\sim 10^{14}$ G, the accretion rate reduces to $\sim 10^{17.5}$ g s^{-1} . And for NGC 300 ULX1, the $B - \dot{M}$ relation with the detected P and \dot{P} is plotted in the blue solid line in the same figure: if the magnetic field of NGC 300 ULX1 is $\sim 10^{12}$ G, the accretion rate is about $\sim 10^{19.7}$ g s^{-1} . When the magnetic field rises up to $\sim 10^{14}$ G, the accretion rate is slightly higher than $\sim 10^{19}$ g s^{-1} . The two accretion rates correspond to the luminosity of $\sim 9.4 \times 10^{39}$ erg s^{-1} and $> 2.0 \times 10^{39}$ erg s^{-1} , where the later one is closed to the observed value of 4.7×10^{39} erg s^{-1} . Thus we suggest that the magnetic field of NGC 300 ULX1 is about $\sim 10^{14}$ G, which will be investigated further in the following sections.

2.2 The magnetic field deduced by the GL model

During the accretion, the total torque N on the NS is $N = I\dot{\Omega}$ for neglecting the typically small effect of the change in the effective

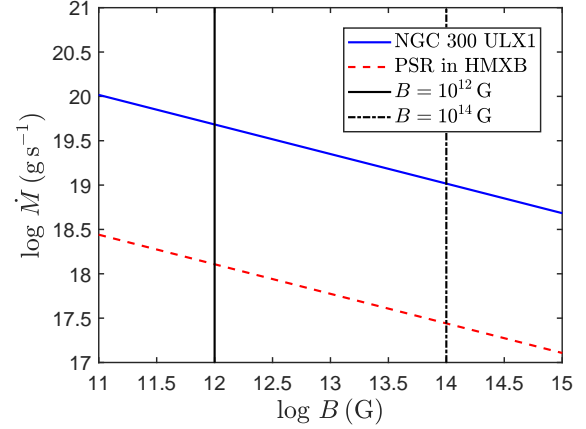


Figure 1. Relation of B and \dot{M} . Tracks of the normal PSR in HMXB and NGC 300 ULX1 are plotted in the red dotted and blue solid lines.

moment of inertia. It can also be expressed in terms of the accretion torque N_{acc} (Ghosh & Lamb 1979; Ghosh 1995):

$$N = n(\omega_s) N_{\text{acc}} \approx n(\omega_s) \dot{M} \sqrt{GMR_0}, \quad (4)$$

where R_0 denotes the transition zone, that is composed of a broad outer zone where the angular velocity is Keplerian and a narrow boundary layer where it departs significantly from the Keplerian value. It is preferred to be $\sim 0.5R_A$. The parameter $n(\omega_s)$ is the dimensionless torque related to the fastness parameter ω_s (Ghosh & Lamb 1979)

$$n(\omega_s) \approx 1.4 \times \left(\frac{1 - \omega_s/\omega_c}{1 - \omega_s} \right), \quad (5)$$

$$\omega_s = 1.19 P^{-1} \dot{M}_{17}^{-3/7} \mu_{30}^{6/7} m^{-5/7}, \quad (6)$$

where \dot{M}_{17} is \dot{M} in units of 10^{17} g s^{-1} , ω_c is the the critical fastness at which the torque changes direction and is taken to be 0.35 (Ghosh & Lamb 1979; Ghosh 1995). In case of $\omega_s < \omega_c$, the PSR is spun up. And for $\omega_s > \omega_c$, the PSR is spun down (Ghosh 1995).

According to equation (4), the spin-up rate is (Ghosh & Lamb 1979)

$$-\dot{P} \approx 5.0 \times 10^{-5} \mu_{30}^{2/7} m^{-3/7} R_6^{6/7} I_{45}^{-1} P^2 L_{37}^{6/7} n(\omega_s) \text{ s yr}^{-1}. \quad (7)$$

In the follow calculation, we take the mass and radius of NGC 300 ULX1 to be the typical values of a standard NS, that are $m = 1.4$ and $R_6 = 1$.

The pulse profile of NGC 300 ULX1 is found to be almost sinusoidal, and dose not appear to be strong beamed (Carpano et al. 2018). Moreover, the accretion rate of the source was detected to be almost constant from 2016 to 2018 (Vasilopoulos et al. 2019). Thus we consider L_{acc} equals to L_X during the field strength calculation. Applying $P = 31.6$ s and $\dot{P} = 5.56 \times 10^{-7}$ s s^{-1} into equation (7), the magnetic field of NGC 300 ULX1 is confound when ω_s is considered in two cases:

- ω_s is assumed to be zero for a slow rotator, and the dimensionless torque is $n(\omega_s) \approx 1.4$, as defined by equation (5) (Ghosh 1995; Parfrey et al. 2016). The estimated magnetic field is $B_1 = 1.19 \times 10^{13}$ G, which is slightly stronger than the works by Carpano et al. (2018) and Vasilopoulos et al. (2018).
- ω_s is determined by equation (6) which is associated with the calculated magnetic field, spin period and luminosity. The inferred

Table 1. The magnetic field of NGC 300 ULX1 estimated with common parameters.

B (G)	ω_s	R_A (cm)
$B_1 = 1.19 \times 10^{13}$	~ 0	1.75×10^8
$B_2 = 3.89 \times 10^{14}$	~ 0.25	1.29×10^9

Notes. Magnetic fields strength are evaluated according to equation (7) with the employed parameters, that are $L_X = 4.7 \times 10^{39}$ erg s $^{-1}$, $P = 31.6$ s and $\dot{P} = -5.56 \times 10^{-7}$ s s $^{-1}$ (Carpano et al. 2018). During the calculation, the field results depend on the dimensionless torque $n(\omega_s)$ associated with ω_s . The Alfvén radius R_A are derived by the deduced magnetic fields.

magnetic field is $B_2 = 3.89 \times 10^{14}$ G and $\omega_s \sim 0.25$, that indicates NGC 300 ULX1 is a highly magnetized NS.

We list the inferred magnetic field B and the corresponding Alfvén radius R_A in Table 1. The co-rotation radius R_{co} is 1.68×10^9 cm for $P = 31.6$ s according to $R_{co} = (GM/4\pi^2)^{1/3} P^{2/3}$. Both of the deduced magnetic fields by GL method imply the relations of $R_A < R_{co}$ and $\omega_s < \omega_c$. These results illustrate that the source is spinning up during the accretion, that is consistent with the observed case of NGC 300 ULX1.

More observations of NGC 300 ULX1 have been performed after it was confirmed as a PULX (Vasilopoulos et al. 2018). Similar to the above calculation, we calculate magnetic fields by 15 pairs of P and \dot{P} that are taken from Table B.1 in Vasilopoulos et al. (2018), as can be seen in Table 2. Vasilopoulos et al. (2018) suggested that the datasets, marked with the symbol “*” from the 2014 *Chandra* and *Swift*/XRT observations, were with gaps and low statistics and therefore resulted in large uncertainties for determining the spin periods and spin-up rates. The magnetic fields inferred from those observed parameters are with the same symbol “*”. The mean value of the field solutions are $B_1 \sim 10^{13}$ G with $n(\omega_s) \simeq 1.4$ for the PSR as a slow rotator, and $B_2 \sim 3.0 \times 10^{14}$ G with $n(\omega_s)$ according to equation (5). In Table 2, both B_1 and B_2 show a weak decay tendency in 3.4 yrs time span of the observation. In order to estimate a rational solution for NGC 300 ULX1, we perform a long term field decay analysis and compare the resulting field estimate with the magnetic field values in Table 2 inferred from observations.

3 THE EVOLVED SIMULATION

3.1 Evolution of the magnetic field

Evolution of NS magnetic field during the accretion has been widely studied and discussed (Bisnovaty-Kogan & Komberg 1974; Geppert & Urpin 1994; van den Heuvel & Bitzaraki 1995; Melatos & Phinney 2000; van den Heuvel 2009; Ho 2011; Igoshev & Popov 2015; Igoshev et al. 2021). For estimating a reasonable magnetic field of NGC 300 ULX1 from the inferred solutions, we will simulate the magnetic field decay along with the accretion time T_{ac} by employing the model of the accretion induced the magnetic field decay of a NS by Zhang & Kojima (2006), hereafter ZK model. It had been used to test the magnetic field evolution of binary pulsars (BPSRs) (Pan et al. 2015).

The ZK model assumes that the PSR is evolved with a constant accretion rate in the accretion. Since the accreted material flows from the polar to the equator, the magnetic field lines in the polar caps are pushed aside and the polar-field strength are diluted. As the PSR magnetosphere is compressed onto the star surface with the accumulation of the accretion material, the accretion might become all over the star and the magnetic field of the PSR decays to the

bottom field. The analytic solution of the evolved magnetic field is Zhang & Kojima (2006):

$$B = \frac{B_f}{\{1 - [C/\exp(y) - 1]^2\}^{7/4}}, \quad (8)$$

where $B_f \simeq 1.32 \times 10^8 (\dot{M}/\dot{M}_{Edd})^{1/2} m^{1/4} R_6^{-5/4} \phi^{-7/4}$ G, is the bottom magnetic field, $\dot{M}_{Edd} \simeq 1.0 \times 10^{18}$ g s $^{-1}$ is the typical Eddington accretion rate of a NS with a mass of $1.4M_\odot$ and radius of 10 km, ϕ is assumed to be 0.5, denoting the ratio of the magnetosphere radius to the Alfvén radius. $C = 1 + [1 - (B_f/B_0)^{4/7}]^{1/2}$, B_0 is the initial magnetic field when the PSR begins the evolution. The parameter $y = 2\xi\Delta M/7M_{cr}$, where $M_{cr} \sim 0.2M_\odot$ is the crust mass, $\Delta M = \dot{M}T_{ac}$ is the accreted material. The parameter ξ ($0 \leq \xi \leq 1$) is the efficiency factor to express the frozen flow of the magnetic line due to the plasma instability. In this work, we assume $\xi = 1$ for the completely frozen field lines that totally drift with the accreted material. The model illustrates that the field evolution of the NS is mainly affected by \dot{M} and T_{ac} .

During the evolution of B with T_{ac} , the initial magnetic field B_0 of NGC 300 ULX1 should be equaled to or stronger than the deduced magnetic field that are listed in Table 2. And \dot{M} is assumed to be a constant corresponding to $L_X = 4.7 \times 10^{39}$ erg s $^{-1}$. It should be noted that the observation time does not mean the accretion time. Hence, we plot the $B - T_{ac}$ relation to find part of the evolved track, which has a similar distribution to the observed B in a time span of 3.4 yrs. After testing different values of B_0 , two $B - T_{ac}$ tracks with $B_0 \sim 3.0 \times 10^{15}$ G for B_1 and B_2 are explored, that couple with the PSR positions well. The accretion time for the source field decaying from B_0 to the deduced value are ~ 4000 yrs for B_1 and ~ 400 yrs for B_2 , as shown in the $B - T_{ac}$ diagram in Fig. 2. The left panel displays the evolved track and the PSR positions with B_1 , and the right panel reveals the ones with B_2 . The sub-figure in each panel is the enlarged image for showing the detailed matching of the evolved track and positions. The red and black solid dots are the $B - T_{ac}$ positions whose magnetic fields are with and without symbol “*” in Table 2, respectively. We see that the $B - T_{ac}$ positions in the right panel are on or closed to the evolved track more tightly than that in the left panel. Moreover, the reduced chi-square of the simulated and calculated magnetic field are ~ 45 for B_1 and ~ 2 for B_2 , which also supports the higher magnetic field of NGC 300 ULX1. So we propose that the magnetic field of NGC 300 ULX1 would be $\sim 3 \times 10^{14}$ G rather than $\sim 10^{13}$ G.

3.2 The evolved results

With the preferred magnetic field strength $B \sim 3.0 \times 10^{14}$ G of NGC 300 ULX1, the B-P evolution is studied according to equations (7) and (8). We first consider a simple case that the source has been experiencing a steady accretion with the defined accretion time and rate. The accretion time is assumed to be the Hubble time 1.38×10^{10} yr (Planck Collaboration et al. 2016). And the accretion rate is with two limitations: the maximum value corresponds to its ultra luminosity $L_X = 4.7 \times 10^{39}$ erg s $^{-1}$. And the minimum value is $\dot{M}_{min} \simeq 4.6 \times 10^{15}$ g s $^{-1}$, which is also the minimum accretion rate required for a MSP forming in the binary system (Pan et al. 2018). The corresponding bottom magnetic fields are $B_{f,max} \simeq 1.73 \times 10^9$ G and $B_{f,min} \simeq 2.34 \times 10^7$ G, respectively. Under these conditions, the B-P evolution began with $B \simeq 3.0 \times 10^{14}$ G and $P = 31.6$ s are shown in Fig. 3, where the blue dotted and dashed lines are with \dot{M}_{max} and \dot{M}_{min} . We find that NGC 300 ULX1 will evolve to be a MSP if the source kept accreting throughout the Hubble time.

Table 2. The magnetic fields of NGC 300 ULX1 deduced with more observed properties

No.	Observatory/ ObsID ^a	T_{obs}^b MJD	P_{Zero}^c s	$\text{Log}(\dot{P})^d$ s s ⁻¹	B_1 10 ¹² G	B_2 10 ¹⁴ G	ω_s
1	C-16029	56978.6	126.28 ^(*)	-4.94 ^(*)	29.16 ^(*)	0.31 ^(*)	0.01 ^(*)
2	S-00049834005	57502	44.18 ^(*)	-6.0 ^(*)	8.86 ^(*)	6.32 ^(*)	0.28 ^(*)
3	N-30202035002	57738	31.718	-6.257	11.36	3.93	0.26
4	X-0791010101	57739	31.683	-6.25	12.12	3.89	0.25
5	X-0791010301	57741	31.588	-6.25	12.37	3.86	0.25
6	S-00049834008	57860	26.87 ^(*)	-6.34 ^(*)	18.59 ^(*)	2.80 ^(*)	0.23 ^(*)
7	S-00049834010	57866	26.65 ^(*)	-6.4 ^(*)	12.14 ^(*)	3.06 ^(*)	0.24 ^(*)
8	S-00049834013	57941	24.24 ^(*)	-6.8 ^(*)	0.94 ^(*)	3.54 ^(*)	0.31 ^(*)
9	S-00049834014	57946	24.22 ^(*)	-6.5 ^(*)	10.59 ^(*)	2.75 ^(*)	0.25 ^(*)
10	S-00049834015	58143	20.06 ^(*)	-6.5 ^(*)	1.58 ^(*)	2.71 ^(*)	0.29 ^(*)
11	N-90401005002	58149	19.976	-6.74	5.90	2.34	0.26
12	C-20965	58157	19.857	< -6.7	< 8.43	> 2.18	> 0.25
13	C-20966	58160	19.808	< -6.7	< 8.64	> 2.16	> 0.24
14	C-20965/20966	58157	19.857	-6.82	3.23	2.51	0.28
15	S-00049834019	58221	19.046 ^(*)	-6.6 ^(*)	25.44 ^(*)	1.34 ^(*)	0.17 ^(*)

Notes. ^(a) Observation ID for *XMM-Newton* (X), *Chandra* (C) and *Swift* (S). ^(b) T_{obs} : start day of observation. ^(c) Pulse period. ^(d) Spin-up rate. Magnetic fields inferred from more observed parameters of T_{ac} , P_{Zero} and $\text{Log}(|\dot{P}|)$, that are given by [Vasilopoulos et al. \(2018\)](#). The calculated B_1 is in case of $n(\omega_s) \sim 1.4$ for $\omega_s \sim 0$ and B_2 is with $n(\omega_s)$ associated with ω_s defined by equation (6). Datas marked with symbol “*” can not be determined a unique set of values due to aliasing and multiple possible solutions caused by gaps and low statics of observations. And we mark the deduced magnetic fields with the same symbol.

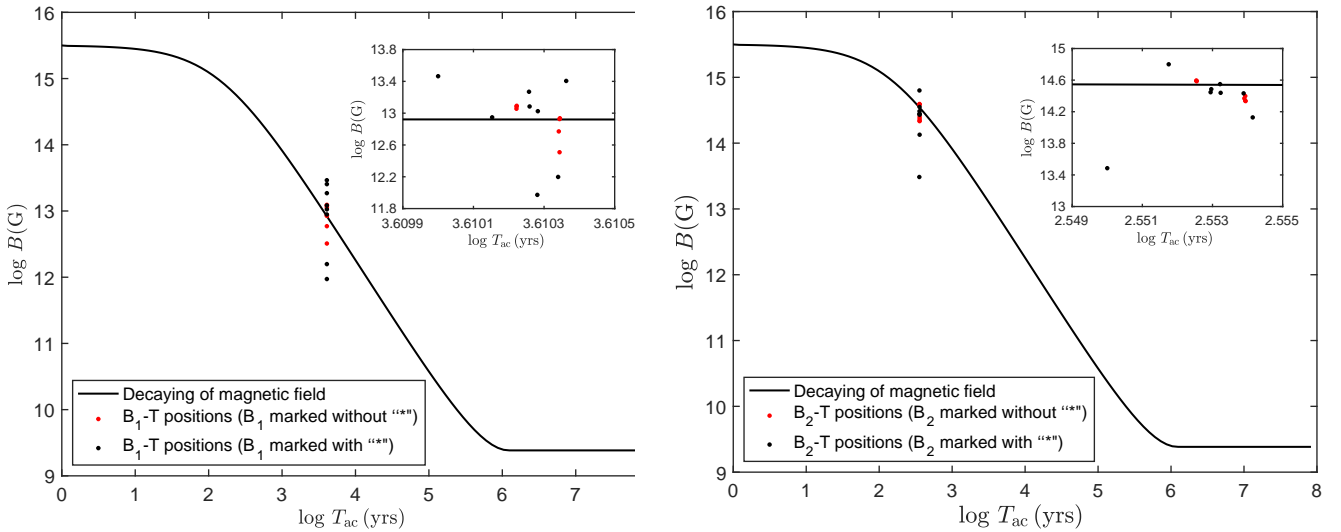


Figure 2. Decaying of the magnetic field of NGC 300 ULX1. We assume that the evolution begins with $T_{\text{ac}} = 0$ and $B_0 \sim 10^{15.5}$ G in two panels. The tracks plotted with the black-solid lines show the the magnetic field decays to the bottom value of $\sim 10^9$ G within about 10^7 yrs. The $B - T_{\text{ac}}$ positions are plotted with the derived values of B_1 and B_2 in Table 2, where the black and red dots are the fields marked with and without symbol “*”, respectively. The enlarged images of the PSR positions to evolved tracks are embedded in two panels.

Since it is hard for a PSR to keep a constant accretion rate during the entire evolution, we now consider that the accretion rate of NGC 300 ULX1 is changeable and fluctuates between \dot{M}_{max} and \dot{M}_{min} . And the source will evolve to different equilibrium status along with the accretion rate variation ([Tong & Wang 2019](#); [Bhattacharya & van den Heuvel 1991](#); [Ho et al. 2014](#)). The accre-

tion time T_{ac} is restricted by the companion mass, which can be inferred from

$$T_{\text{ac}} = 1.3 \times 10^{10} f m_c^{-2.5} \text{ yr}, \quad (9)$$

where m_c is the companion mass in units of solar mass, f is the accreted efficient factor that is usually taken to be 0.1

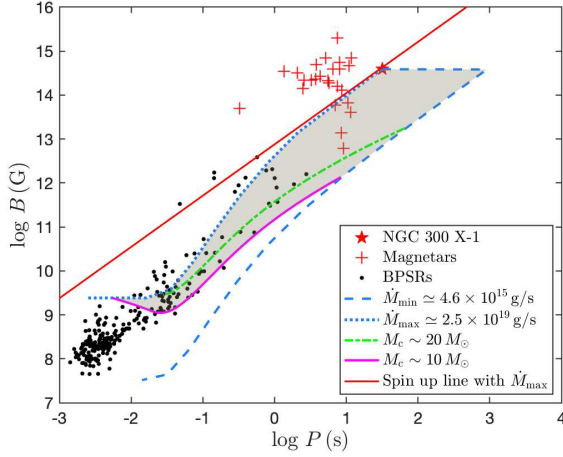


Figure 3. B-P evolved tracks of NGC 300 ULX1. The tracks with the constant accretion rates of $\dot{M}_{\max} \approx 2.5 \times 10^{19} \text{ g s}^{-1}$ and $\dot{M}_{\min} \approx 4.6 \times 10^{15} \text{ g s}^{-1}$ are plotted with the blue dotted and blue dashed lines. The area in grey is the evolutionary range of the source, which is limited by the evolved tracks determined by the variate accretion rate and the companion mass (green dash-dotted line for $M_c = 20 M_\odot$ and magenta solid line for $M_c = 10 M_\odot$). Red star is the B-P position of NGC 300 ULX1 with $B = 3.89 \times 10^{14} \text{ G}$ and $P = 31.6 \text{ s}$. Crossings and solid dots mean the B-P positions of the radio-loud magnetars and the binary pulsars, respectively.

(Shapiro & Teukolsky 1983). It has been detected NGC 300 ULX1 is with a $< 20 M_\odot$ companion (Carpano et al. 2018; Binder et al. 2020). And we consider a lower mass limit of the companion to be $\sim 10 M_\odot$ as it is in HMXB. The corresponding accretion time is $\sim 10^6 - 10^7 \text{ yrs}$ according to equation (9), with the variation of the accretion rate and the accretion time, two evolved B-P tracks are shown in Fig. 3, where the magenta solid line and green dot-dashed line are plotted with $T_{\text{ac}} \sim 10^6 - 10^7 \text{ yrs}$. Now we see that NGC 300 ULX1 evolves to a MSP whose spin period is $\sim 10 \text{ ms}$.

Restricted by three B-P tracks that are the blue dotted line, blue dashed line and magenta solid line (for $M_c = 10 M_\odot$) or green dot-dashed line (for $M_c = 20 M_\odot$), an evolved range of NGC 300 ULX1 is got, that is covered in grey in Fig. 3. It shows all evolved possibilities of NGC 300 ULX1, e.g., a MSP with $B \sim 10^9 \text{ G}$, or an evolved PSR with P about tens of seconds and $B \sim 10^{10} \text{ G}$.

4 DISCUSSIONS

4.1 Comparison with other works

By the $B - \dot{M}$ relation and the GL model, we deduced the magnetic field of NGC 300 ULX1 with the X-ray luminosity, 15 pairs of the observed spin periods and spin-up rates. During the calculation with the GL method, we find that the magnetic field is strongly depends on the fastness parameter ω_s in the GL model. For ω_s defined by equation (6), $B \sim 3.0 \times 10^{14} \text{ G}$. It is consistent with the work by Erkut et al. (2020), who estimated the maximum range of the magnetic dipole field to be $(45 - 240) \times 10^{13} \text{ G}$ from the spin-up rate. And in case of a slow rotator ($\omega_s \sim 0$), $B \sim 10^{13} \text{ G}$, that is closed to the results of $\sim (0.7 - 10) \times 10^{12} \text{ G}$ by Carpano et al. (2018) and $\sim (3 - 20) \times 10^{12} \text{ G}$ by Vasilopoulos et al. (2018).

The field strength $\sim 10^{13} \text{ G}$ of NGC 300 ULX1 is excluded according to the evolution of the magnetic field decaying with the accretion time and the chi-square test for the simulated and the cal-

culated magnetic fields. Based on these study, we conclude that the magnetic field of NGC 300 ULX1 is $\sim 3.0 \times 10^{14} \text{ G}$, and suggest the fastness parameter ω_s to be a variate instead of a constant during the magnetic field deduction.

4.2 Magnetic field constrained by CRSF

CRSF is a direct way for constraining the magnetic field of a PSR. In the confirmed PULXs, M51 ULX8 is the only source that was detected with a certain absorption feature at $\sim 4.5 \text{ keV}$. It was preferred to be with a proton CRSF which implied a magnetic field of $\sim 10^{15} \text{ G}$ (Brightman et al. 2018). NGC 300 ULX1 is the second PULX that was probed a potential CRSF at $\sim 13 \text{ keV}$ based on the phase-resolved broadband spectroscopy using the data of *XMM-Newton* and *NuSTAR*, which implied the magnetic field to be $\sim 10^{12} \text{ G}$ with the assumption of scattering by electrons (Walton et al. 2018). The recent work favored a proton CRSF that could lead to a magnetar field strength of NGC 300 ULX1. It was consistent with the high spin up rate of the source to estimate the plausible ranges for the beaming fraction (Erkut 2021).

Meanwhile, such a CRSF needed a further confirmation, since Koliopanos et al. (2019) found a model without the absorption feature could successfully describe the spectra of NGC 300 ULX1. Therefore, the magnetic field of NGC 300 ULX1 has to be derived through the theory models, such as the accretion torque or the model of the magnetic field decay by accretion. And We look forward to an undoubtable detection of CRSF to determine the magnetic field of NGC 300 ULX1 directly.

4.3 Relations to magnetars

Limited by the accretion rate and accretion time, NGC 300 ULX1 will evolve to an recycled PSR, whose magnetic field is $\lesssim 10^{12} \text{ G}$ and the spin period is $\lesssim 10 \text{ s}$, as shown with the grey area in the B-P diagram in Fig. 3. We plot the B-P positions of magnetars and binary PSRs in the same figure, whose data are from McGill Online Magnetar Catalog and ATNF pulsar catalogue (Manchester et al. 2005; Olausen & Kaspi 2014). It is found that: (1) the present position of NGC 300 ULX1 is closed to the magnetars, (2) its possible B-P evolved area covers not only the magnetars with low magnetic field ($\sim 10^{12} \text{ G}$), but also the gap between magnetars and BPSRs.

It is known that the magnetars are always found as the isolated PSRs whose magnetic field are $\sim 10^{14} - 10^{15} \text{ G}$ (Olausen & Kaspi 2014; Popov 2016; Kaspi & Beloborodov 2017). And there were also a few magnetars whose magnetic field is slightly weaker $\sim 10^{12} \text{ G}$, that were suspected to undergo the accretion induced their fields decay (Rea et al. 2010; Zhou et al. 2014; Mereghetti et al. 2015; Esposito et al. 2021). Meanwhile, there is no binary magnetar found until now. Although an accreted magnetar was doubtful existed in the γ -ray binary system LS 5039 with a period of $\sim 9 \text{ s}$ (Yoneda et al. 2020). It was denied later since the statistical significant bursts or quasiperiodic variability was not found with the same data (Volkov et al. 2021). If NGC 300 ULX1 is the accreting magnetar, it might provide us a chance for probing the magnetar evolution and explaining the formation of the magnetars with the low magnetic fields.

4.4 Ultra X-ray luminosity

Our work suggests that NGC 300 ULX1 is an accreting magnetar whose magnetic field is about $3.0 \times 10^{14} \text{ G}$, which would be with

even more strong multi-pole magnetic field. The strong magnetic field can reduce the electron scattering cross-section of the PSR, and in turn supports the super-critical accretion and ultra X-ray luminosity to occur.

The ultra X-ray luminosity of PULXs can be accounted for by the beaming effect (King & Lasota 2020; Song et al. 2020). However, some confirmed PULXs showed nearly sinusoidal pulse profile which means the beaming effect is negligible. Mushtukov et al. (2021) also suggested that the large pulsed fraction of PULXs excluded the strong beaming (Eksi et al. 2015; Fürst et al. 2017; Carpano et al. 2018). Since NGC 300 ULX1 was observed with a similar property (Carpano et al. 2018), we propose that the accretion luminosity is indeed super-Eddington.

5 CONCLUSIONS

In this paper, we study the magnetic field strength of NGC 300 ULX1 to be $\sim 3.0 \times 10^{14}$ G with the assumption that the source is undergoing a constant accretion rate. Since the pulse profile of NGC 300 ULX1 is almost sinusoidal, the beaming effect is ignored. The B-P evolved simulation, which is confined by the accretion time and accretion rate, shows the source can evolve to a recycled PSR, for instance, a MSP with $B \sim 10^9$ G or an evolved BPSR with $P < 10$ s and $B \sim 10^{10}$ G.

Taking into account the resulting 3.0×10^{14} G field following the accretion induced decay of an initial $\sim 3.0 \times 10^{15}$ G field, we propose NGC 300 ULX1 is probably an accreting magnetar. We also suggest there might be other magnetars among other PULXs such as M82 X-2, NGC 7793 P13 and NGC 5907 ULX (Pan et al. 2016; Israel et al. 2017; Fürst et al. 2017; Tong & Wang 2019). These PULXs can be probed to study the magnetar evolution and the MSP formation in binary systems.

ACKNOWLEDGEMENTS

We would like to thank Liming Song, Na Wang and Qingzhong Liu for helpful discussions. YP, ZL and CZ are supported by National Natural Science Foundation of China (12130342, U1938107, U1838111, U1838117).

DATA AVAILABILITY

The data underlying this article will be shared on reasonable request to the corresponding author.

REFERENCES

Bachetti M., et al., 2014, *Nature*, **514**, 202
 Bachetti M., Grefenstette B. W., Walton D. J., Fuerst F., Heida M., Kennea J. A., Lau R., 2018, *The Astronomer's Telegram*, **11282**, 1
 Bhattacharya D., van den Heuvel E. P. J., 1991, *Phys. Rep.*, **203**, 1
 Binder B. A., Carpano S., Heida M., Lau R., 2020, *Galaxies*, **8**, 17
 Bisnovatyi-Kogan G. S., Komberg B. V., 1974, *Soviet Ast.*, **18**, 217
 Brightman M., et al., 2018, *Nature Astronomy*, **2**, 312
 Carpano S., Haberl F., Maitra C., Vasilopoulos G., 2018, *MNRAS*, **476**, L45
 Dall'Osso S., Perna R., Stella L., 2015, *MNRAS*, **449**, 2144
 Eksi K. Y., Andac I. C., Cikintoglu S., Gencali A. A., Gungor C., Oztekin F., 2015, *MNRAS*, **448**, L40
 Erkut M. H., 2021, *European Journal of Science and Technology*, **27**, 74
 Erkut M. H., Eksi K. Y., Alpar M. A., 2019, *ApJ*, **873**, 105

Erkut M. H., Türkoğlu M. M., Eksi K. Y., Alpar M. A., 2020, *ApJ*, **899**, 97
 Esposito P., Rea N., Israel G. L., 2021, in Belloni T. M., Méndez M., Zhang C., eds, *Astrophysics and Space Science Library* Vol. 461, *Astrophysics and Space Science Library*. pp 97–142 ([arXiv:1803.05716](https://arxiv.org/abs/1803.05716)), [doi:10.1007/978-3-662-62110-3_3](https://doi.org/10.1007/978-3-662-62110-3_3)
 Feng H., Soria R., 2011, *New Astron. Rev.*, **55**, 166
 Fürst F., Walton D. J., Stern D., Bachetti M., Barret D., Brightman M., Harrison F. A., Rana V., 2017, *ApJ*, **834**, 77
 Geppert U., Urpin V., 1994, *MNRAS*, **271**, 490
 Ghosh P., 1995, *Journal of Astrophysics and Astronomy*, **16**, 289
 Ghosh P., Lamb F. K., 1979, *ApJ*, **234**, 296
 Ho W. C. G., 2011, *MNRAS*, **414**, 2567
 Ho W. C. G., Klus H., Coe M. J., Andersson N., 2014, *MNRAS*, **437**, 3664
 Igoshev A. P., Popov S. B., 2015, *Astronomische Nachrichten*, **336**, 831
 Igoshev A. P., Popov S. B., Hollerbach R., 2021, *Universe*, **7**, 351
 Israel G. L., et al., 2017, *Science*, **355**, 817
 Kaspi V. M., Beloborodov A. M., 2017, *ARA&A*, **55**, 261
 King A., Lasota J.-P., 2016, *MNRAS*, **458**, L10
 King A., Lasota J.-P., 2020, *MNRAS*, **494**, 3611
 Kluzniak W., Lasota J. P., 2015, *MNRAS*, **448**, L43
 Koliopoulos F., Vasilopoulos G., Buchner J., Maitra C., Haberl F., 2019, *A&A*, **621**, A118
 Liu J., Di Stefano R., 2008, *ApJ*, **674**, L73
 Liu Q. Z., van Paradijs J., van den Heuvel E. P. J., 2006, *A&A*, **455**, 1165
 Liu Q. Z., van Paradijs J., van den Heuvel E. P. J., 2007, *A&A*, **469**, 807
 Manchester R. N., Hobbs G. B., Teoh A., Hobbs M., 2005, *AJ*, **129**, 1993
 Melatos A., Phinney E. S., 2000, in Kramer M., Wex N., Wielebinski R., eds, *Astronomical Society of the Pacific Conference Series* Vol. 202, IAU Colloq. 177: Pulsar Astronomy - 2000 and Beyond. p. 651
 Mereghetti S., Pons J. A., Melatos A., 2015, *Space Sci. Rev.*, **191**, 315
 Miller J. M., Fabian A. C., Miller M. C., 2004, *ApJ*, **614**, L117
 Mushtukov A. A., Portegies Zwart S., Tsygankov S. S., Nagirner D. I., Poutanen J., 2021, *MNRAS*, **501**, 2424
 Olausen S. A., Kaspi V. M., 2014, *ApJS*, **212**, 6
 Pan Y. Y., Song L. M., Zhang C. M., Guo Y. Q., 2015, *Astronomische Nachrichten*, **336**, 370
 Pan Y. Y., Song L. M., Zhang C. M., Tong H., 2016, *MNRAS*, **461**, 2
 Pan Y. Y., Zhang C. M., Song L. M., Wang N., Li D., Yang Y. Y., 2018, *MNRAS*, **480**, 692
 Parfrey K., Spitkovsky A., Beloborodov A. M., 2016, *ApJ*, **822**, 33
 Planck Collaboration et al., 2016, *A&A*, **594**, A13
 Popov S. B., 2016, *Astronomical and Astrophysical Transactions*, **29**, 183
 Rea N., et al., 2010, *Science*, **330**, 944
 Roberts T. P., Middleton M. J., Sutton A. D., Mezcua M., Walton D. J., Heil L. M., 2016, *Astronomische Nachrichten*, **337**, 534
 Shao Y., Li X.-D., 2015, *ApJ*, **802**, 131
 Shapiro S. L., Teukolsky S. A., 1983, *Journal of the British Astronomical Association*, **93**, 276
 Song X., Walton D. J., Lansbury G. B., Evans P. A., Fabian A. C., Earnshaw H., Roberts T. P., 2020, *MNRAS*, **491**, 1260
 Tong H., 2015, *Research in Astronomy and Astrophysics*, **15**, 517
 Tong H., Wang W., 2019, *MNRAS*, **482**, 4956
 Vasilopoulos G., Haberl F., Carpano S., Maitra C., 2018, *A&A*, **620**, L12
 Vasilopoulos G., Petropoulou M., Koliopoulos F., Ray P. S., Bailyn C. B., Haberl F., Gendreau K., 2019, *MNRAS*, **488**, 5225
 Volkov I., Kargaltsev O., Younes G., Hare J., Pavlov G., 2021, *ApJ*, **915**, 61
 Walton D. J., et al., 2018, *ApJ*, **857**, L3
 Yoneda H., Makishima K., Enoto T., Khangulyan D., Matsumoto T., Takahashi T., 2020, *Phys. Rev. Lett.*, **125**, 111103
 Zhang C. M., Kojima Y., 2006, *MNRAS*, **366**, 137
 Zhou P., Chen Y., Li X.-D., Safi-Harb S., Mendez M., Terada Y., Sun W., Ge M.-Y., 2014, *ApJ*, **781**, L16
 van den Heuvel E. P. J., 2009, in Colpi M., Casella P., Gorini V., Moschella U., Possenti A., eds, *Astrophysics and Space Science Library* Vol. 359, *Physics of Relativistic Objects in Compact Binaries: From Birth to Coalescence*. p. 125, [doi:10.1007/978-1-4020-9264-0_4](https://doi.org/10.1007/978-1-4020-9264-0_4)
 van den Heuvel E. P. J., Bitzaraki O., 1995, *A&A*, **297**, L41

This paper has been typeset from a $\text{\TeX}/\text{\LaTeX}$ file prepared by the author.